Volume 1 | Number 1 | Jan 2013 | Pages 1–100

Journal of
Materials Chemistry C

Materials for optical and electronic devices
www.rsc.org/materialsC

ROYAL SOCIETY
OF CHEMISTRY

ROYAL SOCIETY
OF CHEMISTRY

www.rsc.org/materialsC

Journal of Materials Chemistry C

Dynamic Article Links ▶

ARTICLE

Tunable Charge Transport through n-ZnO nanorods on Au coated Macroporous p-Si

Arpita Jana,[a] Siddhartha Ghosh,[b] P. Sujatha Devi,[c] Nil Ratan Bandyopadhyay[a] and Mallar Ray[a],*

We report a strategy to synthesize patterned n-ZnO nanorods on Au coated macroporous p-Si. Electric field assisted growth of ZnO under UV exposure results in the formation of well-aligned and relatively defect free n-ZnO nanorods on the macroporous Si-template. The luminescence characteristics of ZnO exhibit a single Gaussian peak due to band-to-band transition in ZnO. Temperature dependent electrical
10 transport through the n-ZnO/Au/p-Si heterojunction reveals unusual characteristics. Under forward bias, the *I-V* plots are diode-like with a remarkably low turn-on voltage and significantly high forward bias current. The non-linear forward current decreases appreciably with temperature while the reverse bias current is linear and is almost temperature independent. The Au layer present between the n-ZnO and p-Si significantly modifies the junction and allows tuning the device characteristics from diode like to Ohmic
15 under different biasing conditions.

Introduction

ZnO based nanostructures have attracted substantial research attention owing to their unique optical and electrical characteristics.[1-4] Applications of ZnO nanorods have already
20 been demonstrated in high gain photodetectors,[5] light emitting diodes (LEDs),[6] sensors,[7] solar cells,[8] UV lasers,[9] and piezoelectronics.[10] Most of these devices rely on ZnO nanorod based heterojunctions that are grown/deposited on various types of substrates. Since Si remains the building block of present day
25 microelectronics, investigation of ZnO nanorods grown/deposited on Si substrate is of fundamental importance for integrating the exciting properties of ZnO nanostructures with existing Si technology. Consequently, ZnO/Si hybrid nano-systems, particularly n-ZnO/p-Si heterojunctions, have been well-
30 explored.[11] In this regard, two issues still pose major challenges in making these devices amenable for real-life applications. First, synthesis of large scale, defect free ZnO nanorods utilizing room temperature deposition technique has remained a difficult problem.[12] In addition, the transfer of as-grown random
35 networked ZnO nanorods onto the desired substrate has been one of the most challenging tasks.[13] In this communication, we address the above issues by a simple synthetic strategy. A cost-effective technique involving electric field assisted growth, results in the formation of well-aligned and patterned n-ZnO
40 nanorods on Au coated macroporous p-Si templates in a scalable proportion. The photoluminescence (PL) characteristic of the hybrid system exhibits a single Gaussian peak suggesting the formation of relatively defect free ZnO nanorods.
Potential applications of ZnO nanorod based heterojunctions

45 require understanding of the electrical properties of the device at different temperatures. Consequently, temperature dependent electrical transport through n-ZnO/p-Si heterojunctions has been widely investigated.[14-17] Since, the presence of amorphous SiO_2 layer on the Si surface inhibits the growth of ZnO directly on Si,
50 different buffer layers such as MgO/TiN,[18] AlN-MgO/TiN,[19] GaN,[20] yttria-stabilized zirconia,[21] ZnS,[22] Y_2O_3,[23] and recently graphene,[24] have been used to integrate ZnO with Si substrates. Most of these devices exhibit conventional rectifying behaviour with very high ideality factors and low breakdown voltages.
55 However, there has been no report about the heterojunction behaviour of n-ZnO/p-Si with Au as a buffer layer. Au nanostructures are extremely promising candidates for molecular-scale interconnects in nanoelectronic devices.[25] Additionally, the choice of thin Au buffer layer offers two more advantages. First,
60 Au prevents ambient oxidation of the etched Si templates which produces the unwarranted insulating barrier of SiO_2[26]. Second, Au is reported to act as a catalyst that promotes vertical alignment of ZnO nanorods grown on substrates.[27] It is therefore important to understand the transport mechanism of n-ZnO/Au/p-
65 Si heterojunction based devices and their behaviour at different temperatures prior to their adoption in the fabrication of nanodevices.
In the present study we demonstrate that the electrical transport properties of the heterojunction in presence of the interfacial Au
70 layer between the n-ZnO and p-Si is significantly modified by the metallic electrons. Contrary to previous reports we see that the device exhibits diode like characteristics with remarkably low turn-on voltage and high forward current under forward bias and nearly Ohmic transport under reverse bias condition. This

This journal is © The Royal Society of Chemistry [2014]

J. Mater. Chem. C, 2014, **[vol]**, 00–00 | **1**

phenomenon allows tuning the device characteristics from diode like to Ohmic under different biasing conditions.

Experimental

Macroporous Si templates with uniform pore distribution were formed on high resistivity (ρ=10 Ω-cm), p-type Si wafers in a specially designed teflon bath by anodic etching in HF and N,N-dimethylformamide (DMF) solution. The detail of the formation procedure is discussed elsewhere.[28, 29, 30] Electro-polished Si wafers were etched for 1.5 h in a solution of HF/DMF (ratio – 1:9) under a constant current density (J) of 5 mA/cm^2. The as-prepared macroporous templates were treated with 10% buffered HF to etch the native oxide layer and dried under N_2. The sample was immediately introduced inside a sputter coating unit (Hitachi E1010) and the top surface was coated with Au for 30 s. Ohmic contacts were established on the backside of the macroporous template by e-beam deposition of Ag-Al followed by annealing at 700°C for 45 s.[28] The Au coated macroporous Si templates were used as substrates for growth of ZnO nanorods by chemical solution route using 0.0375 M zinc acetate. Ammonia solution was added drop wise to maintain the pH at 9. The details of ZnO nanorod growth has been discussed in ref. 31. In an attempt to electrically align the ZnO nanorods, the reaction and thermal treatment were carried out in a teflon bath using a Pt electrode as a cathode and the macroporous template as the anode. A current field of 100 mA/cm^2 was applied throughout the reaction and the sample was irradiated with intense UV (60 W, 265 nm Hg lamp) with an intention to charge the growing n-ZnO nanorods so that the growth direction is preferentially driven along the direction of the applied field. After completion of the reaction, the solution was allowed to cool and the macroporous template was taken out and rinsed with DI-water. Two reference samples: (i) a colloidal suspension of n-ZnO nanorods and (ii) n-ZnO on Au coated, electropolished Si wafer were prepared using the same parameters and under exactly similar experimental conditions. The morphology of the macroporous Si templates and the deposited ZnO nanorods were investigated by field emission scanning electron microscopy (FE-SEM) using a Zeiss (Carl Zeiss Microscopy Ltd, Sigma 02-87) and a Hitachi 3400 N SEM. The PL spectra of the samples were recorded in the wavelength range of 345-630 nm by exciting the samples with a wavelength of 325 nm (determined by PL excitation study) using a Horiba Jobin Yvon, Flurolog-3 (Nanolog) spectrofluorometer (Model FL3) fitted with a 450 W xenon lamp. Temperature dependent (80-300 K) current-voltage (I-V) characteristics were recorded by a Janis ST-500 under flowing N_2 environment. Metallic contacts were fabricated, using a shadow mask, on the ZnO rods by e-beam deposition (Varian) of 600 nm thick and 0.5 mm diameter pads of Ag which were subsequently annealed at 300°C for 30 s (supplementary information).

Results and discussion

Figures 1(a)-(d) show representative SEM images of the as-prepared macroporous Si, n-ZnO nanorods on electropolished p-Si grown in absence of applied field, and ZnO nanorods grown on macroporous p-Si templates under the influence of external electric field. It is clear from Fig. 1 (a) that the macroporous Si template consists of more-or-less uniform pores running parallel to each other (inset panel, Fig. 1a). The average pore diameter and the depth are estimated to be ~1.3 µm and 3 µm, respectively. The ZnO nanorods grown on un-etched, Au coated Si wafers shown in Fig. 1 (b) shows sign of vertical alignment but majority of the tapered rods remain arbitrarily tilted. Average length and diameter of the rods are ~1 µm and 500 nm, respectively. A significant improvement in alignment of well distributed ZnO on the Si surface is observed in Fig. 1 (c). It is interesting to note that the individual rods have assembled into a flower like morphology under the applied field. We are inclined to believe that the formation of branched flower like structures from rods is due to the polarity driven assembly of the individual rods under an electric field — a phenomenon which we are currently investigating.
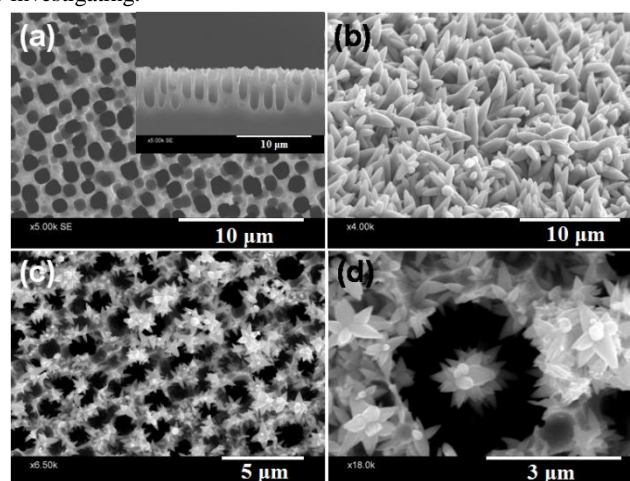
Fig. 1 SEM images showing (a) macroporous Si with well-distributed pores (J=5 mA/cm^2, t=1.5 h, HF:DMF=1:9). Inset panel shows that the pores are nearly parallel. (b) Quasi-aligned ZnO rods on Au coated Si wafer formed without external bias; (c) well-aligned and patterned ZnO nanorods on macroporous template under the influence of external field; and (d) growth of vertical ZnO nanorods inside a pore.

Although most of the ZnO seem to grow on the Si pillars standing between the pores, a closer scrutiny reveals that ZnO nanorods have also grown inside the pores as evident from Fig. 1 (d). The applied field coupled with UV exposure, therefore, affects an alignment of ZnO structures in between and within the pores giving rise to the formation of patterned ZnO nanorods on macroporous Si coated with Au. The tickness of the Au layer on the macroporous Si is ~24 nm (supplementary information).

Journal of Materials Chemistry C

ARTICLE
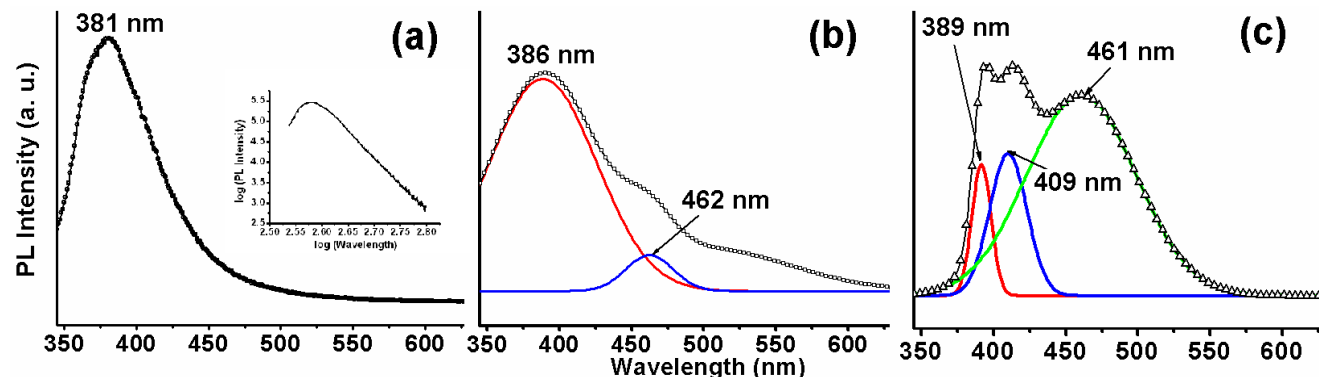
Fig. 2 Room temperature PL spectra of (a) ZnO rods on Au coated macroporous Si grown under the influence of electric field and UV. Inset is the log-log plot; (b) ZnO rods on Au coated electropolished p-Si wafer under UV exposure; and (c) colloidal ZnO nanorods synthesized under identical conditions without external field. The excitation energy in each case was 325 nm. The spectra in (b) and (c) are de-convoluted by fitting appropriate multiple Gaussian curves.

The first striking feature of the ZnO nanorods grown on macroporous template is evident from the PL spectra shown in Figs 2 (a)-(c) which were recorded in the wavelength range of 345-630 nm by exciting the samples with a wavelength of 325 nm. The spectrum of ZnO nanorods on macroporous Si is characterized by a single Gaussian peak centred around 381 nm (Fig. 2a). Log-log plot of this profile shown as inset of Fig. 2 (a) does not reveal any sign of additional peaks. Figs 2 (b) and (c) show the PL characteristics of the reference samples prepared on Au coated Si and colloidal suspensions, respectively. These samples were prepared using exactly the same protocol, but without an applied field. The dramatic difference between the three PL curves indicate the following: (i) strong UV emission peaks at 381, 386 and 389 nm, respectively, are due to excitonic recombination corresponding to the band edge emission (bandgap of ZnO is 3.37 eV); (ii) the presence of double peaks in Fig. 2 (b) shows that ZnO on Au coated electropolished Si have oxygen vacancy related defects;[32] (iii) the same ZnO nanorods in colloids show two additional and more intense peaks at 409 nm (Zn interstitial),[33] and at 461 nm (single ionized oxygen vacancy defect);[31] and (iv) most importantly the absence of any other peak in Fig. 2 (a) strongly suggest that the ZnO on macroporous Si appears to be free of defects as far as room temperature spectroscopic signal is concerned. Therefore, we conclude that electric field in conjunction with UV exposure produces relatively defect free ZnO rods on Au coated macroporous Si templates. At this stage we tentatively assign this phenomenon to the annihilation of defecs by electric field and possible splitting of water under the influence of UV and electric field which has a strong influence to produce defect free ZnO nanorods.[34]

In ZnO nanoparticles oxygen adsorbed on the surface captured electron forms negatively charged ions[35]. This leads to upward band bending near the surface.[36] In presence of higher energy light the photogenerated holes migrate along the band and react with negatively charged oxygen ions. This increases the conductivity and plays an important role in both electric and optoelectric properties. From the PL emission characteristics it is observed that the ZnO rods are spectroscopically defect free as there is no peak related to the oxygen vacancies. It has been widely observed that ZnO nanoparticles having oxygen vacancy defect forms an O_2^- ion by capturing an electron from conduction band.[37, 38] This leads to a scarcity of electrons in the conduction band of ZnO nanoparticle which decreases the electrical performance.[39] But in our case the ZnO nanorods are nearly defect free. So the possibility of deterioration in electrical performance in this process is negligible. Eventually by this fabrication route we are getting improved and tunable device characteristics that is discussed later. It is well understood that in ZnO rods electronic charges are generated in a great amount in the presence of the UV light.[40, 41] Now, when we introduce these charged ZnO rods in an electric field the crystalline growth is found to be almost defect free and regularly aligned. This is because when positive voltage is applied, H^+ are annihilated by the negatively charged ZnO rods and negative OH^- easily resides on the surface of the growth region of the ZnO nanorods. The accumulated negative charges fill up the positively charged oxygen vacancy (defect) and reduce the signature peak of oxygen related defect in visible PL emission.[42] Although, this aspect of defect annihilation requires more in depth study, we believe that the dramatic absence of defect related peak in the sample is essentially due to this effect which we are presently investigating in details. In addition, we do not rule out the possible splitting of water under UV exposure, which also assists the formation of relativly defect free ZnO nanorods.[34]

It may be noted here that we attempted to grow ZnO nanorods on the macroporous Si template so as to demonstrate a structure where the ZnO are firmly embedded within the pores thereby producing a robust system. However, as of now we see that most

This journal is © The Royal Society of Chemistry [2014]

J. Mater. Chem. C, 2014, **[vol]**, 00–00 | **3**

of the ZnO nanorods grow on Si deposits outside the pores. Nevertheless, these ZnO structures are firmly attached to the porous template as the samples were thoroughly rinsed in alcohol prior to characterization. Of course a structure where the ZnO
5 nanorods grow inside the pores is favorable but for the purpose of the present study we proceed with this heterogeneously distributed but aligned ZnO nanorods as we see that irrespective of whether the ZnO grows inside or outside the pores, the entire system is highly depleted of defects and fairly robust.
10 In an attempt to understand the collective charge transport though the n-ZnO/Au/p-Si heterostructure, temperature dependent (80-300 K) current-voltage (*I-V*) characteristics were recorded under flowing N$_2$ environment. Metallic contacts were fabricated, using a shadow mask, on the ZnO rods by e-beam deposition of Ag
15 which were subsequently annealed at 300°C for 30 s. A schematic of the device set up for *I-V* measurements is shown in Fig. 3. It may noted here that the Ag/Al back contact shown in Fig. 3 was used for the fabrication of macroporous Si template and for applying the field during the growth of ZnO nanorods and not
20 used for *I-V* measurements.
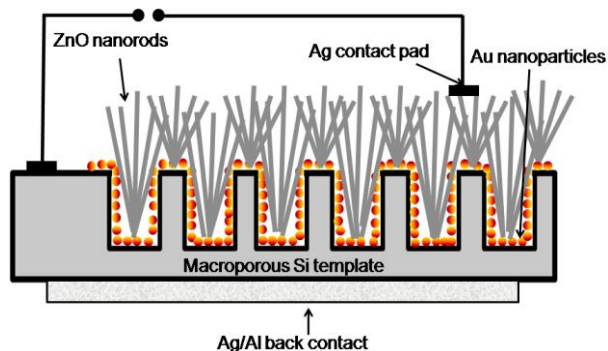
Fig. 3 Schematic of the n-ZnO/Au/p-Si heterojunction.

Fig.4 *I-V* characteristics of n-ZnO and p-Si heterojunction with a thin Au
25 layer sandwiched between them at temperatures ranging from 80 to 300 K. Left-upper inset shows the excellent fit of the forward bias current with the ideal diode equation for two extreme temperatures, 80 and 300 K. Left-lower inset shows the turn on voltages, determined by extrapolating the linear fits in the high current regimes at 80 and 300 K.
30 Right-lower inset is the log-log *I-V* plots of the device at two typical temperatures indicating two distinct regions dependent on the applied bias voltage.

From Fig. 4, we see that the *I-V* curves of the device exhibit

unusual characteristics where the forward bias current varies non-
35 linearly with voltage, while under reverse bias condition the variation is nearly Ohmic. Here, we note that our device essentially consists of n-ZnO and p-Si with a thin Au layer sandwiched between them, which forms two back-to-back Schottky junctions in series. The forward bias characteristics of
40 the heterojunction is very well described by the ideal diode equation:

$$I = I_0 \left[\exp\left(q \frac{V - V_{th}}{\eta k T} \right) - 1 \right] \qquad (1)$$

where *I*o is the saturation current, *q* is the electronic charge, V_{th} is the threshold voltage, *k* is the Boltzmann constant, *T* the absolute
45 temperature and η is the diode ideality factor. The excellent fit of the curves to the above equation is shown in the left-upper inset, Fig. 4 for the two extreme temperatures, 80 and 300 K. The device is characterized by a remarkably low turn-on voltage (0.11 V at room temperature) and significantly high forward bias
50 current. At 15 V the forward current varies from 65.45 to 87.9 mA for temperature varying from 80 to 300 K, whereas the turn-on voltage, determined by extrapolating the linear fits in the high current regimes (left-lower inset panel, Fig. 4), varies between 0.17 to 0.11 V for the same temperature range. These values are
55 significantly better than the data reported earlier for different types of ZnO nanorod based devices.[43, 44] The reverse bias current is high (-31.5 mA for -15 V sweep) and is almost temperature independent. The forward current, on the other hand, decreases appreciably with decreasing temperature. Such characteristics
60 may be explained in terms of tunnelling through a barrier out of occupied levels whose population is modified by the nonzero temperature, and a potential barrier that allows increased penetration with increasing forward voltage.[45] The presence of the Au layer with supply of free charge carriers reduces the built-
65 in-potential which consequently increases the reverse current and significantly lowers the turn-on voltage.

The right-lower inset panel, Fig. 4 shows the log-log *I-V* plots of the device under forward bias at two typical temperatures. The plot clearly exhibits two distinct regions dependent on the applied
70 bias voltage. In region I, when the bias is <1.0 V, the current varies linearly with voltage, irrespective of the temperature, whereas in region II (bias>1.0 V), the variation is exponential. Hence, the transport mechanism of our device is apparently dominated by tunneling at lower voltages (region I) and
75 recombination-tunneling at higher voltages (region II).[46] Strikingly, unlike previous reports dealing with similar ZnO based diodes,[46, 47] space-charge-limited current conduction is absent in our device. This is because the Au layer separating the n-ZnO and p-Si delimits the space-charge region by allowing
80 easy migration of free electrons and lowering the built-in-voltage, both under forward as well as reverse bias conditions.
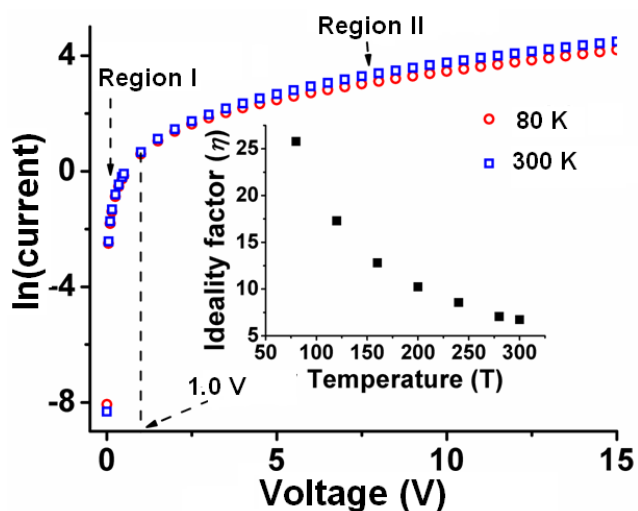
Fig.5 Variation of ln(I) versus V of the n-ZnO/Au/p-Si heterojunction showing two different regions determined by bias voltage for 80 and 300 K. The inset panel is the variation of the diode ideality factor (η) with temperature, for bias< 1.0 V

The existence of two different regions is further illustrated in the ln(current) versus voltage plots shown in Fig. 5. The diode ideality factor (η), describing the deviation of the diode from an ideal one is evaluated from the plots for the two different regions. Interestingly, we see that η is substantially high and strongly dependent on temperature. In region I, i.e. for bias <1.0 V, η varies from ~6.7 to 25.8 (shown as inset, Fig. 5) whereas for bias > 1.0 V, giant values of η ranging from ~150 to 650 for temperature variation from 300 to 80 K, are obtained. The device therefore is not a conventional Schottky diode. High ideality factor ($\eta > 2$) is a very common feature observed in high bandgap heterojunctions and is usually attributed to defects,[46] effect of high doping,[48] image force lowering of Schottky barrier at the interface,[49] and generation-recombination currents within the space-charge region.[49] According to Wen et al.[50] high ideality factor is attributed to a bias voltage dependent Schottky barrier height. All these models assume spatially homogeneous, flat interface between metal and semiconductor that deviates any diode from an ideal one.[51] However, the ZnO nanorods in our case are more-or-less defect free, both ZnO and Si have very low dopant concentration, and the Au layer delimits the space-charge region. Consequently, it is not possible to account for such giant η values by any of these models. Brötzmann et al.[52] showed that for series arrangements of Schottky junctions, Frenkel–Poole type resistance, and an Ohmic contact resistance, η approaches giant values (>100) which is due to interfacial disorder and/or due to presence of an amorphous layer. We propose that the presence of interfacial disordered Au layer, separating the crystalline p-Si and n-ZnO, contributes to such colossal η values and provides experimental support to the model proposed by Brötzmann et al.[52] Nevertheless, η values of our device at room temperature for bias < 1.0 V is very close to recently reported values for ZnO based heterojunctions.[47] The decrease in ideality factor with increasing temperature is the well-known T_0 effect and may be attributed to the effect of image force.[46] The role of thermionic field emission and enhanced tunneling in addition to image force cannot be completely ruled out in explaining the temperature dependence of η at this stage of investigation.

From the above discussion it is clear that the existence of the Au layer between n-ZnO and the macroporous p-Si remarkably modifies the junction and its corresponding electrical properties. A simplified band diagram of the device is shown in Fig. 6, where two back-to-back Schottky junctions are formed. The band structure of the isolated components are shown in the top panel of Fig. 6 (a). Under unbiased condition, the bandgap (Eg) for n-ZnO and p-Si are 3.37 and 1.12 eV, respectively and their respective electron affinities (χ) are 4.35 and 3.95 eV, respectively.[53] The work function of Au is taken to be 4.82 eV.[54] The bottom panel of Fig. 6 (a) is the equilibrium band structure where the Fermi level (E_F) is a constant, leading to a built-in-voltage across the junction that is strongly affected by the presence of Au layer. The top and the bottom panels of Fig. 6 (b) show the schematic of the band under forward and reverse bias respectively. $E_{F,p\text{-}Si}$ and $E_{F,n\text{-}ZnO}$ here are the majority-carrier quasi-Fermi levels of p-Si and n-ZnO, respectively. Now, proper rectification in Schottky junctions is expected when $\Phi_M > \Phi_S$ for n-type semiconductors and $\Phi_M < \Phi_S$ for p-type semiconductors, where Φ_M and Φ_S are the workfunctions of metals and semiconductors, respectively.[24] Although these conditions are satisfied in our device we do not see a significant blocking effect under reverse bias condition. This is because the effective concentration of the minority carriers (electrons) in p-Si is significantly increased due to diffusion of electrons from the adjacent Au layer thereby resulting in a large reverse bias current that varies almost linearly with the biassing voltage. The effect is more pronounced in our device since we have used a high resistivity Si wafer with low concentration of majority carriers. n-ZnO on the other hand has a larger concentration of majority carriers compared to p-Si which accounts for diode like forward characteristics of the device with low turn-on voltage.

The optical and transport properties of our device are in keeping yet significantly different from that of similar heterojunction nanostructures. The absence of defect related transition in the PL spectrum and swithing from typical diode like to Ohmic transport, simply by reversing the bias, are unique features of our system. Similar ZnO-Si based heterojunctions with metallic buffer layers investigated before have exhibited enhanced PL, but the defect related transition signatures were almost ubiquitiously present. The transport characteristics of these systems usually exhibited typical diode like characteristics both under forward and reverse bias. For example a thin (~10 nm) amorphous Al_2O_3 layer deposited in between ZnO and p-Si, was reported to enhance PL intesity and decrease the reverse leakage current due to insulating properties of Al_2O_3. However, the I-V charateristics showed typical diode like behavior with low threshold and the PL spectrum clearly had defect related peaks.[55] ZnO used as buffer layer in an n-ZnO/p-Si heterojunction exhibited room temperature electroluminescence due to radiative recombination through deep-level defects, while diode-like electrical transport was attributed to tunneling mechanism via deep-level states.[56] PL spectrum of ZnO/Si heterojunction with an AlN buffer layer also exhibited strong excitonic peak along with very weak defect-related deep level visible emissions.[57] Introduction a thin layer of NiO between the n-type ZnO and p-type GaN reportedly increases luminescence efficiencies by blocking electron injections from the ZnO to the GaN side.[58] Kang et al.[59] have

recently shown that inserting a thin (3 nm) amorphous tungsten oxide layer in between ZnO/Si heterojunction of a Si solar cell remarkably reduces the defect density at the Si/ZnO interface, resulting in decreased series and increased shunt resistances. We believe that introduction of Au nanoparticles as a buffer layer in the present study, in a similar manner, dramatically reduces the defect density at the Si/ZnO interface and helps in the growth of spectroscopically defect free ZnO nanorods. It is also reported very recently that Au deposition prevents the growth of SiO_2 on the surface of Si nanostructures.[60] SiO_2 layer produces large number of non-radiative centers at the ZnO/Si interface and results in poor crystallinity of ZnO films.[61] So restriction of SiO_2 growth on the surface of Si is necessary for the formation of good n-ZnO/p-Si heterojunction. Although the exact role of Au buffer layer warrants further investigation, our device characteristics clearly indicate that the presence of such a layer helps in remarkable improvement of the optical spectrum and endows a tunability in the electrical transport.
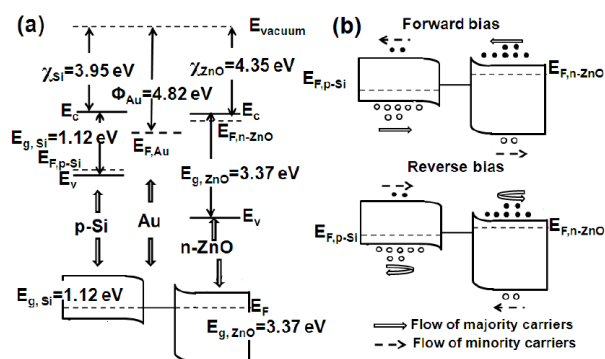
Fig. 6 Simplified schematic of the energy bands of n-ZnO/Au/p-Si heterojunction. (a) individual bands of n-ZnO, Au and p-Si (top panel), and that of the heterojunction under equilibrium (bottom panel); (b) Energy bands and formation of quasi Fermi levels of the device under forward (top panel) and reverse bias (bottom panel) conditions

Conclusions

In conclusion, we have successfully fabricated well aligned and patterned n-ZnO nanorods on Au coated macroporous Si template under UV exposure coupled with externally applied electric field. The PL characteristic of the ZnO nanorods are characterized by a single Gaussian peak that is attributed to band-to-band transitions indicating that the ZnO nanorods are relatively defect free. The temperature dependent *I-V* plots are diode-like under forward bias with a remarkably low turn-on voltage and significantly high forward bias current. There are two distinct regions in the forward characteristics of the heterojunction. Below 1.0 V bias, the current varies linearly with voltage, whereas for bias>1.0 V, the variation is exponential. The diode ideality factor varies by an order of magnitude in the two regions determined by the bias. The non-linear forward current decreases appreciably with temperature while the reverse bias current is linear and is almost independent of temperature. We propose that the Au layer present between the n-ZnO and p-Si significantly modifies the junction and allows tuning the device characteristics from diode like to Ohmic under different biasing conditions. Such heterojunctions with tunable transport properties have important potential applications in electronic and opto-electronic devices.

Notes and references

a School of Materials Science and Engineering, Indian Institute of Engineering Science and Technology, Shibpur, Howrah, India. Fax: +9133 2668 1926; Tel: +91 33 2668 8140; E-mail: mray@matsc.becs.ac.in
b Department of Electrical and Computer Engineering, University of Illinois at Chicago, Chicago 60607, USA. Fax: +1 312 996 6465; Tel: +1 312 996 5256; E-mail: sghosh@ece.uic.edu
c Nano-structured Materials Division, CSIR-Central Glass and Ceramic Research Institute, 196 Raja S. C. Mullick Road, Kolkata 700032, India. psujathadevi@cgcri.res.in

1   M. H. Huang, S. Mao, H. Feick, H. Yan, Y. Wu, H. Kind, E. Weber, R. Russo and P. Yang, *Science*, 2001, **292**, 1897-1899.

2   O. Harnack, C. Pacholski, H. Weller, A. Yasuda and J. M. Wessels, *Nano Lett.*, 2003, **3**, 1097–1101.

3   S. Chu, G. Wang, W. Zhou, Y. Lin, L. Chernyak, J. Zhao, J. Kong, L. Li, J. Ren and J. Liu, *Nature Nanotechnol.*, 2011, **6**, 506–510.

4   S. Y. Park, K. Kim, K. H. Lim, B. j. Kim, E. Lee, J. Ho Chob and Y. S. Kim, *J. Mater. Chem. C*, 2013, **1**, 1383-1391.

5   C. Soci, A. Zhang, B. Xiang, S. A. Dayeh, D. P. R. Aplin, J. Park, X. Y. Bao, Y. H. Lo and D. Wang, *Nano Lett.*, 2007, **7**, 1003-1009.

6   S. N. Das, J. H. Choi, J. P. Kar, K. J. Moon, T. I. Lee and J. M. Myoung, *Appl. Phys. Lett.*, 2010, **96**, 092111.

7   L. Liao, H. B. Lu , J. C. Li , H. He , D. F. Wang , D. J. Fu , C. Liu and W. F. Zhang, *J. Phys. Chem. C*, 2007, **111**, 1900-1903.

8   J. Huang, Z. Yin and Q. Zheng, *Energy Environ. Sci.*, 2011, **4**, 3861-3877.

9   H. Dong, Y. Liu, J. Lu, Z. Chen, J. Wang and L. Zhang, *J. Mater. Chem. C*, 2013, **1**, 202-206.

10   S. M. Kim, J. I. Sohn, H. J. Kim, J. Ku, Y. J. Park, S. N. Cha and J. M. Kim, *Appl. Phys. Lett.*, 2012, **101**, 013104

11   X.-M. Zhang, D. Golberg, Y. Bandoa and N. Fukata, *Nanoscale*, 2012, **4**, 737-741.

12   S. K. Park, J. H. Park, K. Y. Ko, S. Yoon, K. S. Chu, W. Kim and Y. R. Do, *Cryst. Growth Des.*, 2009, **9**, 3615–3620.

13   M. Y. Bae, K. W. Min, J. Yoon, G.-T. Kim and J. S. Ha, *J. Appl. Phys.*, 2013, **113**, 084310.

14   C. W. Cao, W. N. Bao, X. Lin, X. Y. Liu, Y. Geng, H. L. Lu, Q. Q. Sun, P. Zhou, D. W. Zhang and P. F. Wang, *ECS Solid State Letters*, 2013, **2**, Q25-Q28.

15   S. Chirakkara and S. B. Krupanidhi, *Thin Solid Films*, 2012, **520**, 5894–5899.

16   S. H. Park, S. H. Kim and S. W. Han, *Nanotechnology*, 2007, **18**, 055608.

17   J. D. Ye, S. L. Gu, S. M. Zhu, W. Liu, S. M. Liu, R. Zhang, Y. Shi and Y. D. Zheng, *Appl. Phys. Lett.*, 2006, **88**, 182112.

18   Y. W. Zhang, X. M. Li, W. D. Yu, X. D. Gao, Y. F. Gu, C. Yang, J. L. Zhao, X. W. Sun, S. T. Tan, J. F. Kong and W. Z. Shen, *J. Phys. D Appl. Phys.*, 2008, **41**, 205105.

19   C. Jin, R. Narayan, A. Tiwari, H. Zhou, A. Kvit and J. Narayan, *Mater. Sci. Eng. B*, 2005, **117**, 348.

20   A. Nahhas, H.K. Kim and J. Blachere, *Appl. Phys. Lett.*, 2001, **78**, 1511.

21   R. Aggarwal, C. Jin, P. Pant, J. Narayan and R. J. Narayan, *Appl. Phys. Lett.*, 2008, **93**, 251905.

22   A. Miyake, H. Kominami, H. Tatsuoka, H. Kuwabara, Y. Nakanishi and Y. Hatanaka, *J. Cryst. Growth*, 2000, **214-215**, 294.

23   W. R. Liu, Y. H. Li, W. F. Hsieh, C. H. Hsu, W. C. Lee, Y. J. Lee, M. Hong and J. Kwo, *Cryst. Growth Des.*, 2009, **9**, 239.

24 Z. Liang, X. Cai, S.O Tan, P. Yang, L. Zhang, X. Yu, K. Chen, H. Zhu, P. Liu and W. Mai, *Phys. Chem. Chem. Phys.,* 2012, **14**, 16111-16114.

25 C. Wang, Y. Hu, C. M. Lieber and S. Sun, *J. Am. Chem. Soc.*, 2008, **130**, 8902-8903.

26 M. Ray, T. S. Basu, N. R. Bandyopadhyay, R. F. Klie, S. Ghosh, S. O. Raja and A. K Dasgupta, *Nanoscale*, 2014, **6**, 2201-2210.

27 X. Wang, J. Song, P. Li, Jae H. Ryou, R. D. Dupuis, C. J. Summers and Z. L. Wang, *J. Am. Chem. Soc*., 2005, **127**, 7920-7923.

28 S. Ghoshal, A. A. Ansar, S. O. Raja, A. Jana, N. R. Bandyopadhyay, A. K. Dasgupta and M. Ray, *Nanoscale Res. Lett.,* 2011, **6**, 540.

29 M. M. Das, M. Ray, N. R. Bandyopadhyay and S. M. Hossain, *Mater. Chem. Phys.,* 2010, **119,** 524.

30 M. Ray, S. Ganguly, M. Das, S. M. Hossain and N. R. Bandyopadhyay, *Comp. Mater. Sci*., 2009, **45**, 60.

31 A. Jana, P. Sujatha Devi, A. Mitra, and N. R. Bandyopadhyay, *Mater. Chem. Phys*., 2013, **139**, 431-436.

32 X. P. Shen, A. H. Yuan, Y. M. Hu, Y. Jiang, Z. Xu and Z. Hu, *Nanotechnology*, 2005, **16**, 2039.

33 A. B. Djurišić, W. C. H. Choy, V. A.L. Roy, Y. H. Leung, C. Y. Kwong, K. W. Cheah, T. K. G. Rao, W. K. Chan, H. F. Lui and C. Surya, *Adv. Func. Mater.*, 2004, **14**, 856-864.

34 B. Meyer, D. Marx, O. Dulub, U. Diebold, M. Kunat, D. Langenberg and C. Woll, *Angew. Chem. Int. Ed*., 2004, **43**, 6641-6645.

35 M. W. Chen, J. R. D. Retamal, C. Y. Chen and J. H. He, *IEEE Electron Device Lett.*, 2012, **33**, 411-413.

36 Q. H. Li, T. Gao, Y. G. Wang and T. H. Wang, *Appl. Phys. Lett.*, 2005, **86**,123117.

37 Q. Wan, Q. H. Li, Y. J. Chen, T. H. Wang, X. L. He, J. P. Li and C. L. Lin, *Appl. Phys. Lett*., 2004, **84**, 3654.

38 L. Liao, H. B. Lu, J. C. Li, H. He, D. F. Wang, D. J. Fu, C. Liu and W. F. Zhang, *J. Phys. Chem. C* 2007, **111**,1900-1603.

39 S. Y. Liu, T. Chen, Y.-L. Jiang, G. –P. Ru and X.-P. Qu, *J. Appl. Phys.*, 2009, **105**, 114504.

40 N. Serpone, D. Lawless and R. Khairutdinovt, *J. Phys. Chem.*,1995, **99**, 16646-16654.

41 B. O'Regan, M. Gratzel and D. Fitzmaurice, *Chem. Phys. Lett.*, 1991, **183**, 89-93.

42 M. Ghosh and A. K. Raychaudhuri, *Appl. Phys. Lett.* 2011. **98**, 153109.

43 X. M. Zhang, M. Y. Lu, Y. Zhang, L. J. Chen and Z. L. Wang, *Adv. Mater.*, 2009, **21**, 2767-2770.

44 S. W. Lee, H. D. Cho, G. Panin and T. W. Kang, *Appl. Phys. Lett*., 2011, **98**, 093110.

45 J. H. He, S. T. Ho, T. B. Wu, L. J. Chen and Z. L. Wang, *Chem. Phys. Lett.,* 2007, **435**, 119-122.

46 N. K. Reddy, Q. Ahsanulhaq, J. H. Kim and Y. B. Hahn, *Appl. Phys. Lett*., 2008, **92**, 043127.

47 D. D. Sang, H. D. Li, S. H. Cheng, Q. L. Wang, Q. Yu and Y. Z. Yang, *J. Appl. Phys.,* 2012, **112**, 036101.

48 R. F. Broom, H. P. Meir and W. Walter, *J. Appl. Phys.,* 1986, **60**, 1832.

49 E. H. Rhoderick and R. H. Williams, Metal–Semiconductor Contacts, 2nd ed. (Clarendon, Oxford, 1988).

50 L. Wen, K. M. Wong, Y. Fang, M. Wub and Y. Lei, *J. Mater. Chem.*, 2011, **21**, 7090-7097.

51 M. Sharma and S. K. Tripathi, *J. Appl. Phys.,* 2012, **112**, 024521.

52 M. Brötzmann, U. Vetter and H. Hofsäss, *J. Appl. Phys.,* 2009, **106**, 063704.

53 F. A. Padovani and G. G. Sumner, *J. Appl. Phys*., 1965, **36**, 3744.

54 K. W. Boer, *Survey of Semiconductor Physics* (Van Nostrand, New York, 1990).

55 T. Wang, H. Wu, C. Chen, and C. Liu, *Appl. Phys. Lett*., 2012, **100**, 011901.

56 J. D. Ye, S. L. Gu, S. M. Zhu, W. Liu, S. M. Liu, R. Zhang, Y. Shi and Y. D. Zheng, *Appl. Phys. Lett.* 2006, 88, 182112.

57 L.S. Chuah, Z. Hassan, S. K. Mohd Bakhori, M. A. Ahmad and Y. Yusof, *Am. J. Nanosc. Nanotechnol.* 2013, **1**, 1-5

58 M. A. Abbasi, Z. H. Ibupoto, M. Hussain and O. Nur, M. Willander, *Nanoscale Res. Lett.* 2013, **8**, 320.

59 S. J. Kang, J.-W. Jeon, S. J. Baik and K. S. Lim, *Appl. Phys. Lett.* 2013, **103**, 153903.

60 T. S. Basu and M. Ray, *J. Phys. Chem. C* 2014, **118**, 5041-5050.

61 J. B. You, X. W. Zhang, S. G. Zhang, H. R. Tan, J. Ying, Z. G. Yin, Q. S. Zhu and P. K. Chu, *J. Appl. Phys.,* 2010, **107**, 083701.
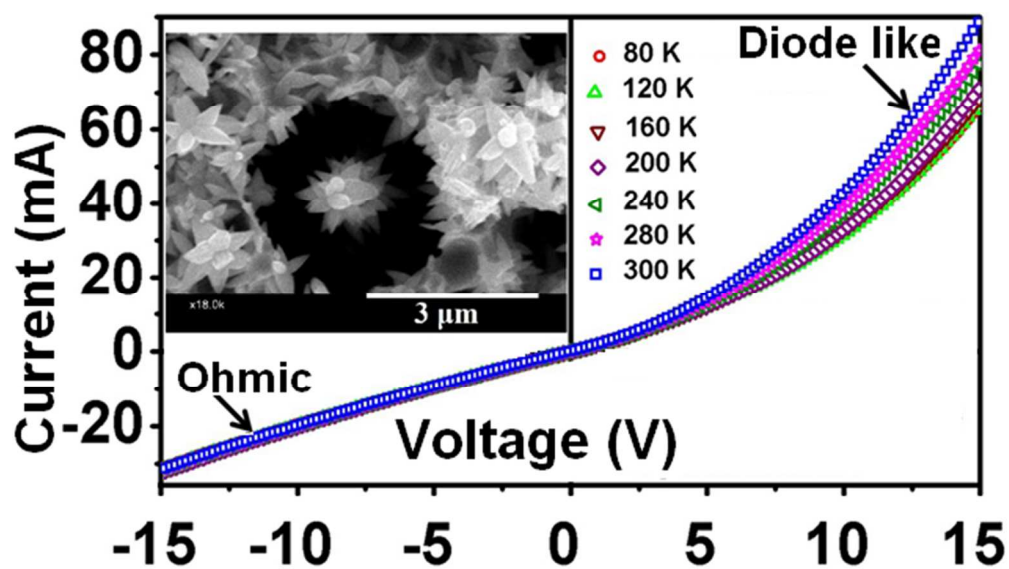
Diode-like and Ohmic charge transport through aligned ZnO nanorods on Au coated macroporous Si
94x53mm (300 x 300 DPI)